Deep-Learning-Based Precipitation Observation Quality Control

YINGKAI SHA,[a] DAVID JOHN GAGNE II,[b] GREGORY WEST,[c] AND ROLAND STULL[a]

[a] The University of British Columbia, Vancouver, British Columbia, Canada
[b] National Center for Atmospheric Research, Boulder, Colorado
[c] BC Hydro, Burnaby, British Columbia, Canada

(Manuscript received 1 June 2020, in final form 18 February 2021)

ABSTRACT: We present a novel approach for the automated quality control (QC) of precipitation for a sparse station observation network within the complex terrain of British Columbia, Canada. Our QC approach uses convolutional neural networks (CNNs) to classify bad observation values, incorporating a multiclassifier ensemble to achieve better QC performance. We train CNNs using human QC'd labels from 2016 to 2017 with gridded precipitation and elevation analyses as inputs. Based on the classification evaluation metrics, our QC approach shows reliable and robust performance across different geographical environments (e.g., coastal and inland mountains), with 0.927 area under curve (AUC) and type I/type II error lower than 15%. Based on the saliency-map-based interpretation studies, we explain the success of CNN-based QC by showing that it can capture the precipitation patterns around, and upstream of the station locations. This automated QC approach is an option for eliminating bad observations for various applications, including the preprocessing of training datasets for machine learning. It can be used in conjunction with human QC to improve upon what could be accomplished with either method alone.

KEYWORDS: Precipitation; Data quality control; Classification; Deep learning; Machine learning

1. Introduction

Precipitation observation quality control (QC) is a long-standing challenge because of its high spatial and temporal variability with skewed intensity spectra: the majority of precipitation observations are close to zero; while rare extreme events can bring abnormally high precipitation values that behave similarly to spurious outliers. On the instrumental side, gauge-based precipitation measurements are biased by both systematic instrumental errors (e.g., splashing/blowing of rain/snow in/out of the gauge, losses due to the aerodynamic effects above the gauge orifice, water adhering to the gauge surface and evaporation) (Goodison et al. 1998; Adam and Lettenmaier 2003; Yang et al. 2005; Rasmussen et al. 2012), and technical or maintenance issues (e.g., mechanical malfunctions, data transmission error; Groisman and Legates 1994).

Sophisticated QC procedures have been carried out in various meteorological and hydrological research projects. These QC procedures are typically a mix of automated examination of internal consistencies (i.e., checks of value range, rate of change, and homogeneity with predefined thresholds) (Meek and Hatfield 1994; Eischeid et al. 2000; Adler et al. 2003; Schneider et al. 2014) and human-based QC with graphical workstations (i.e., displaying precipitation values together with orography and other background fields to determine their quality) (e.g., Xie and Arkin 1996; Jørgensen et al. 1998; Adler et al. 2003; Schneider et al. 2014). Although human-involved QC has reported success in many projects, this approach is resource-intensive and can cause delays when processing a high volume of data (Mourad and Bertrand-Krajewski 2002). Human QC may also bring subjectivity into the quality labels, resulting in a downgrade of data quality.

Many automated observation QC methods have been proposed to reduce the workload of human-based QC, including 1) time series-based anomaly detection (e.g., Mourad and Bertrand-Krajewski 2002; Piatyszek et al. 2000; You et al. 2007), 2) cross validating neighboring stations with geostatistical methods (e.g., Eischeid et al. 1995; Hubbard et al. 2005; Štěpánek et al. 2009; Xu et al. 2014), and 3) bad-value classification with decision trees (e.g., Martinaitis et al. 2015; Qi et al. 2016) and neural networks (Sciuto et al. 2009; Lakshmanan et al. 2007, 2014; Zhao et al. 2018).

In this study, we provide a novel automated QC approach for precipitation observations with deep artificial neural networks (DNNs). We define automated QC as a binary classification problem—that is, classifying each observation with a "good" or "bad" QC flag. The type of DNN applied in this study is a convolutional neural network (CNN). Our CNNs take station precipitation observations, preprocessed gridded precipitation and elevation values centered around each station location as inputs, using human-labeled quality flags as training targets.

Based on the ability of CNNs to learn from gridded data, in this study, we aim to provide an automated QC method that requires less data dependencies. As we will introduce later, this research focuses on gauge data from a specific observation network; however, the potential of generalization and data dependency replacements are also discussed. This is in contrast to many existing QC methods that require a greater number of

Denotes content that is immediately available upon publication as open access.

Corresponding author: Yingkai Sha, yingkai@eoas.ubc.ca

DOI: 10.1175/JTECH-D-20-0081.1

observational data sources and/or ones with greater spatial coverage [e.g., closely located neighboring stations (Maul-Kötter and Einfalt 1998), radar coverage (Martinaitis et al. 2015; Qi et al. 2016)].

Based on the above concepts, we apply the following hypotheses in this research: CNNs are capable of 1) learning representations of precipitation patterns from gridded precipitation input, 2) learning representations of complex terrain conditions from gridded elevation input, and 3) utilizing these representations to classify QC flags. Further, with the above research hypotheses, we address the following research questions: 1) How well can CNNs classify QC flags? 2) What is the role of elevation input in this QC problem? 3) Given the imperfection of gridded precipitation analysis, can we preprocess this input to enable CNNs to learn effective representations? And 4) can we explain the classification behavior of CNNs in this QC problem?

The rest of this paper is organized as follows: section 2 describes the region of interest and data; section 3 introduces methodologies, including the design of CNNs and the automated QC workflows; section 4 evaluates the general classification results and answers research questions 1 and 2; section 5 provides interpretation studies of CNNs and answers research questions 3 and 4; and sections 6 and 7 are the discussion and conclusions.

2. Data

a. Region of interest

The region of interest for this research is British Columbia (BC), Canada. BC is located in southwestern Canada, bordering the northeast Pacific Ocean and has complex geographical conditions. The south coast of BC is a combination of coastal and mountainous environments. Southeastern BC is covered by the Columbia and Rocky Mountains, whereas central and northeastern BC are a mix of flat terrain and mountain ranges (Odon et al. 2018).

Precipitation observation QC is complicated in BC by its complex terrain, which negatively impacts the continuity, reliability, and spatial representativeness of ground-based observations (Banta et al. 2013). Good-quality observations are needed in numerical weather prediction (NWP) operations for postprocessing, verifying, and analyzing the forecast. Excluding bad gauge values to preserve the quality of precipitation observations within BC watersheds is of special importance as hydrology models are sensitive to the station precipitation inputs (e.g., Nearing et al. 2005; Null et al. 2010). Small changes in precipitation can cause large changes in watershed response. Good-quality precipitation observations are fundamental to correctly estimating the hydrological states of these watersheds and to postprocess precipitation forecast inputs.

The main electric utility in BC, BC Hydro, generates more than 90% of its electricity from hydropower, mostly within the watersheds of the Peace (northeastern BC) and Columbia (southeastern BC) River basins (BC Hydro 2020). Reliable hydrological forecasts are critical to the planning and operation of these hydroelectric facilities. Greater automation of the QC process would offer more timely and reliable and less resource-intensive precipitation data in support of this.

b. In situ observations

The in situ observations applied in this research are taken from 80 gauge stations within and near BC Hydro watersheds (Fig. 1a). We divide these watersheds into three regions based on their precipitation regimes: 1) the south coast, directly affected by Pacific frontal cyclone systems in the wet fall, winter, and spring months, with dry summer months (Fig. 1a, blue dots); 2) the southern interior, which sees frequent, but lighter precipitation amounts year-round (Fig. 1a, red dots); and 3) northeast BC, which sees drier winters and wetter summers (Fig. 1a, yellow dots) (e.g., Chilton 1981; Odon et al. 2018).

BC Hydro stations use standpipe- and weighing-bucket-type precipitation gauges; they provide real-time gauge observations as heights with accuracies ranging from 2.0 to 0.05 mm, reporting precisions ranging from 0.1 to 1.0 mm and reporting intervals varying from every 15 min to every 2 h (Table 1; BC Hydro 2019, personal communication). A given station can have different precision and observation frequencies at different times in its period of record. Manual (human) QC is performed on the raw gauge observations with the following steps: 1) Precipitation trends are compared against nearby stations known to have similar precipitation patterns. 2) Precipitation amounts are compared with the Regional Deterministic Precipitation Analysis (described in the following subsection) and with collocated snow pillows. 3) When in doubt, BC Hydro Meteorologists are consulted (BC Hydro 2019, personal communication). Although not perfect, these human QC'd observations are recognized as reliable values in this research, and are used to create quality labels for the supervised training of the automated QC system.

c. Gridded data

We use two gridded datasets: elevation obtained from ETOPO1 (Amante and Eakins 2009) and accumulated 6-h precipitation obtained from the Canadian Regional Deterministic Precipitation Analysis (RDPA).

ETOPO1 is a 1-arc-min resolution global elevation model maintained by the National Geophysical Data Center. ETOPO1 elevation is a key input of our method because orography largely controls the distribution of precipitation over BC.

The Canadian Meteorological Centre (CMC) within Environment and Climate Change Canada (ECCC) produces the Canadian Precipitation Analysis (CaPA), comprised of the Regional and High Resolution Deterministic Precipitation Analyses (RDPA and HRDPA, respectively) (Canadian Centre for Climate Services 2019). The RDPA, used in this study, takes the output of the 10-km Regional Deterministic Prediction System (RDPS) as its background field and has been calibrated with radar products from Canadian Weather Radar Network, and with gauge observations from multiple observational networks (BC Hydro observations are not ingested) through optimum interpolation (OI) (Mahfouf et al. 2007; Fortin et al. 2015). The RDPA data exhibit generally good and homogeneous skill throughout Canada (Lespinas et al. 2015). They outperform

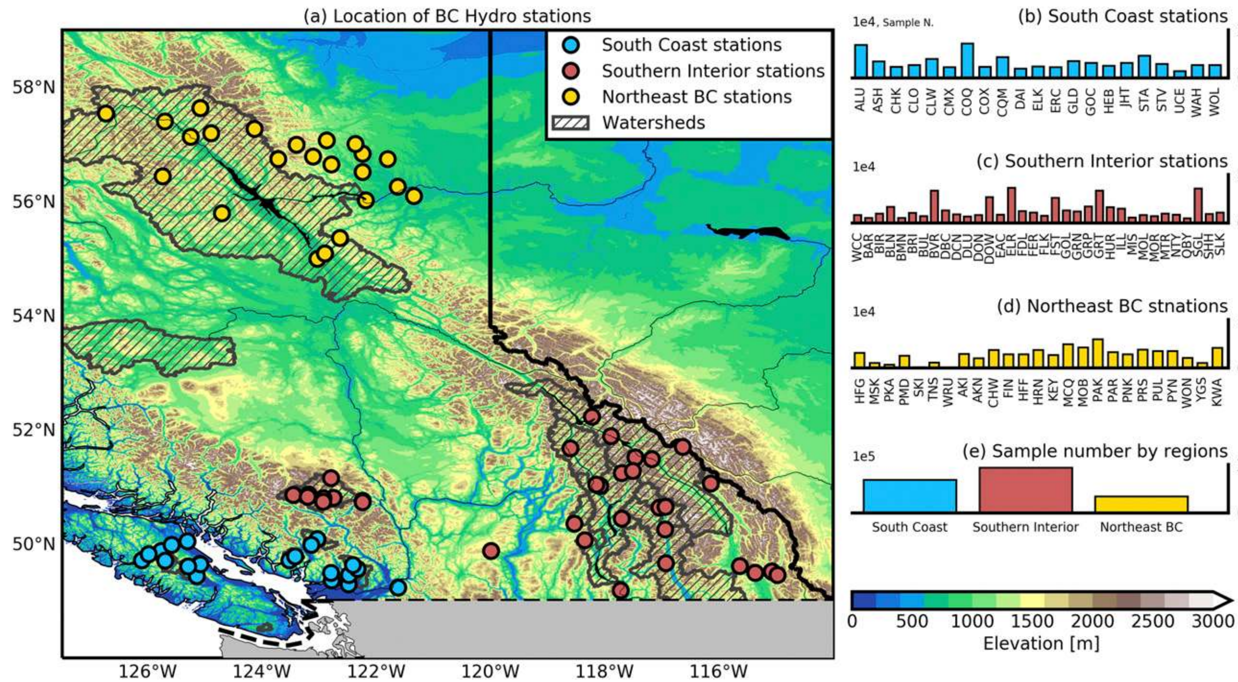

FIG. 1. (a) Locations of BC Hydro precipitation gauge stations as classified into three geographical regions with elevation (color shaded) and watersheds (hatched) as background. (b)–(d) Numbers of nonzero resampled observations from each BC Hydro station in each region after preprocessing. (e) The total number of preprocessed observations in regions in (b)–(d).

their RDPS background field (Lespinas et al. 2015) and several observation only products (Wong et al. 2017; Fortin et al. 2018).

We choose the RDPA data because they have high spatial and temporal resolutions, are available in near–real time, and are an optimized combination of precipitation estimation from numerical model, radar, and station observation data. Additionally, the RDPA covers the entire land territory of Canada, including areas north of 60°N. The gridded precipitation information in the north is a key input for QC'ing stations in northeast BC. Figure 2a provides an example of the RDPA during a precipitation event.

That said, there are caveats to using the RDPA. Coverage of weather-station and radar data ingested into the analysis in BC is mostly in southern BC. Further, several studies have concluded that the RDPA underestimates solid precipitation (e.g., Carrera et al. 2010; Fortin et al. 2018). This is because many precipitation observations and radar data in the cool season are discarded in the RDPA due to a high probability of snow measurement bias (Canadian Centre for Climate Services 2019; ECCC 2019, personal communication). The result is that, outside of the population centers of southern BC, and especially in winter, RDPA values are largely from the RDPS background field. Despite this, it still contains useful information about the likely spatial distribution and magnitude of precipitation. It is best, however, not to use the RDPA to match with BC Hydro station observations on a point-by-point basis, but rather for information about precipitation patterns around the target station.

3. Method

a. The use of gridded data

We use a gridded precipitation analysis (RDPA) as an information source for the spatial distribution of precipitation around a station. We hypothesize that differentiating between no/low precipitation and high precipitation zones is more important than the specific precipitation rate value at a single grid point. However, the quality of gridded precipitation values vary. When a nonzero observation value is within an RDPA

TABLE 1. The product name, gauge types, and parameters of the BC Hydro precipitation gauges. The number of activated stations (No.) is valid for the 2016–18 research period only. An asterisk indicates precision is effective at the BC Hydro side.

Name	Gauge type	Precision	Full scale (FS)	Accuracy	No.
OTT Pluvio 2	Weighing gauge	0.1 mm*	750 mm	0.05 mm	15/80
OTT PLS	Standpipe gauge	1.0 mm	4 m	2 mm (0.05% FS)	33/80
Honeywell Sensotech TJE	Standpipe gauge	0.1 mm*	2 m	2 mm (0.1% FS)	30/80
Belfort Model 6071	Weighing gauge	0.1 mm	750 mm	3.75 mm (0.5% FS)	2/80

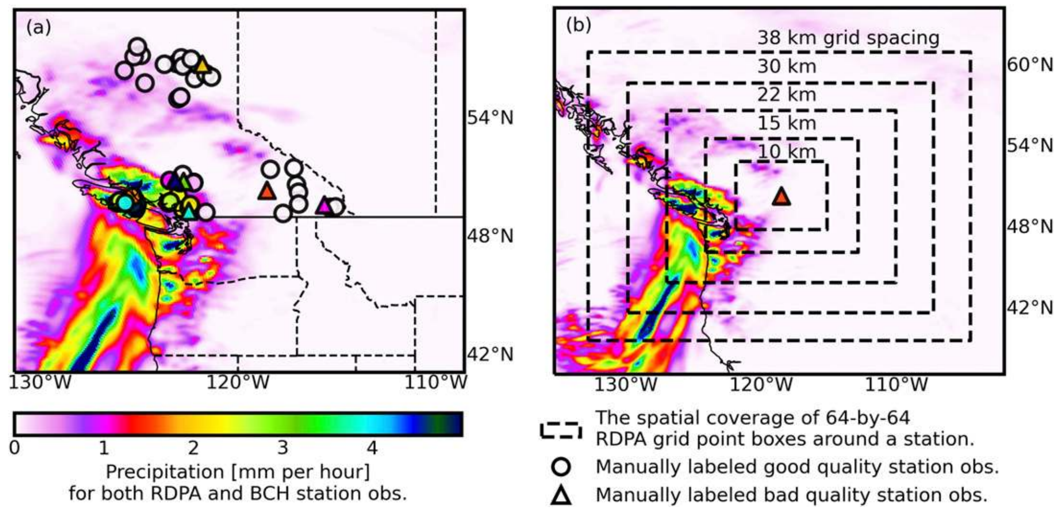

FIG. 2. (a) An example precipitation event. Precipitation values shown are hourly precipitation rates for the 6 h ending 1200 UTC 3 Jan 2016. Color shading is the Regional Deterministic Precipitation Analysis (RDPA), while circled and triangular markers are manually labeled good- and bad-quality BCH observations. (b) As in (a), but with a specific bad observation (color-filled triangle), and spatial coverage of regridded RDPA/ETOPO1 64 × 64 sized inputs (dashed boxes).

high precipitation area, as opposed to a precipitation-free area, it should have a higher chance to be labeled as "good," and vice versa. One example of the above statement is provided in Fig. 2a. In a precipitation event affecting the south coast of BC, two southern interior stations reported nonzero values. These two stations are located in a precipitation-free area, and far from the main precipitation area. The human QC team classified these two observations as unreliable, and corrected them to zero.

To compare observed values to their surrounding precipitation–orography patterns, we crop multiple subsets of grid points from RDPA and ETOPO1 around the location of each station as inputs (Fig. 2b). The effectiveness of the RDPA and ETOPO1 subsets depends on their spatial coverage. Ideally, these subsets should be big enough to cover the precipitation pattern around the target station, and small enough to avoid more remote, irrelevant precipitation systems. Precipitation features of potential importance vary widely due to orographic and synoptic forcings. Here, we consider a range of scales, with the RDPA and ETOPO1 both regridded to roughly 38-, 30-, 22-, 15- and 10-km grid spacings on regular latitude–longitude grids. We take 64 × 64 gridpoint subsets of this regridded RDPA and ETOPO1 data, centered on the location of each station (dashed boxes in Fig. 2b), then replace the centermost 2 × 2 grid points with the raw observation value. QC is performed on each grid spacing separately to consider precipitation information across different spatial scales. We do not downscale RDPA data to finer resolutions since the RDPA is mainly populated by the RDPS model first-guess field around station locations (see section 2c), and this 10-km model cannot resolve features at smaller scales. Further, as will be shown, finer grid spacings perform worse. Details of regridding, cropping, and gridded data-observation matching are summarized in section 3d.

b. CNN-based classifier

We apply CNNs as the QC classification algorithm. CNNs are feedforward DNNs with convolution kernels. Each convolution kernel is a multidimensional array of trainable weights that learns the abstraction of grid-like topology (Goodfellow et al. 2016; Gu et al. 2018). Compared with other neural-network-based algorithms, CNNs are regularized better, for extracting information from gridded data. Within atmospheric science, CNNs have achieved success in weather pattern detection (e.g., Liu et al. 2016), and gridded downscaling (e.g., Vandal et al. 2018).

We use ResNet-like CNNs to build QC classifiers (He et al. 2015a). The ResNet-like architecture combines skip connections and densely stacked hidden layers as identity blocks (Fig. 3), which can solve the vanishing gradient problem in CNN training. Our CNN-based classifier has roughly 50 000 trainable weights with 18 stacked hidden layers. Each hidden layer is a convolutional layer with valid padding, batch normalization (BN) (Ioffe and Szegedy 2015), parametric rectified linear unit (PReLU) (He et al. 2015b) activation function and spatial dropout (Tompson et al. 2015) (Fig. 3).

Our CNN accepts 64 × 64 gridpoint inputs with two channels and produces classification probabilities through a sigmoid kernel. It is trained with a cross-entropy loss function and an adaptive moment estimation (Adam) optimizer (Kingma and Ba 2017). Learning rate decay and early stopping are applied during the training. This QC problem is fully supervised since labels (good, bad) have been assigned manually for all available samples.

c. Classifier ensembles and QC workflow

By training CNN classifiers separately for different grid spacing samples, they can predict QC flags independently.

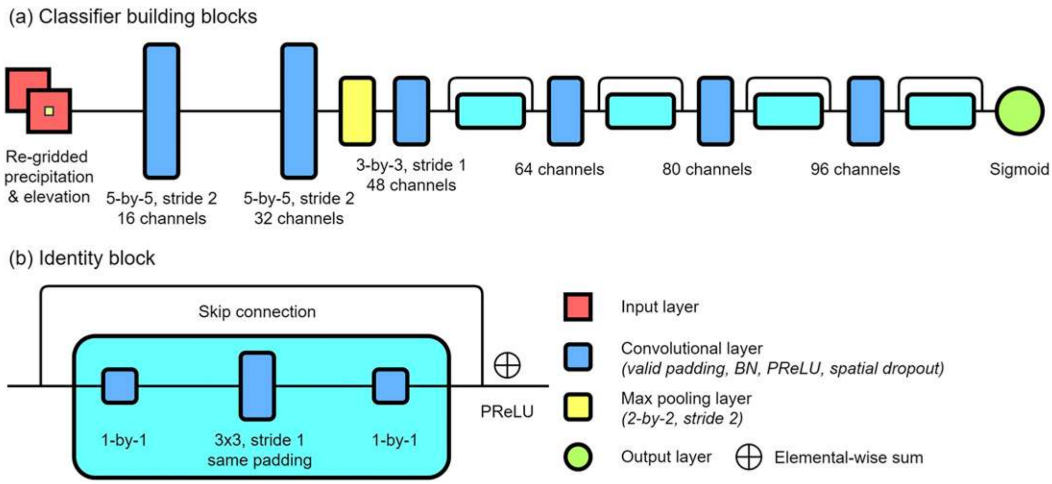

FIG. 3. (a) The design of the CNN classifier and (b) identity blocks. For the convolutional layers that contain identity blocks, batch normalization (BN) and parametric rectified linear unit (PReLU) are calculated before entering an identity block. Spatial dropout is performed at the end of an identity block.

For combining these QC flags into a single probabilistic value, a commonly used approach is ensemble learning (e.g., Jiang et al. 2018). We use a single hidden layer and fully connected artificial neural network [also known as ''multilayer perceptron'' (MLP)] with 10 hidden nodes, hyperbolic tangent activation function, and sigmoid output kernel as the classifier ensemble. Operationally, an automated QC system can be formed by combining all the previous steps into a unified workflow (Fig. 4).

d. Baseline models

For evaluating the actual performance gain of the CNN-based classifiers (hereafter ''main classifiers''), three sets of classification baselines are proposed.

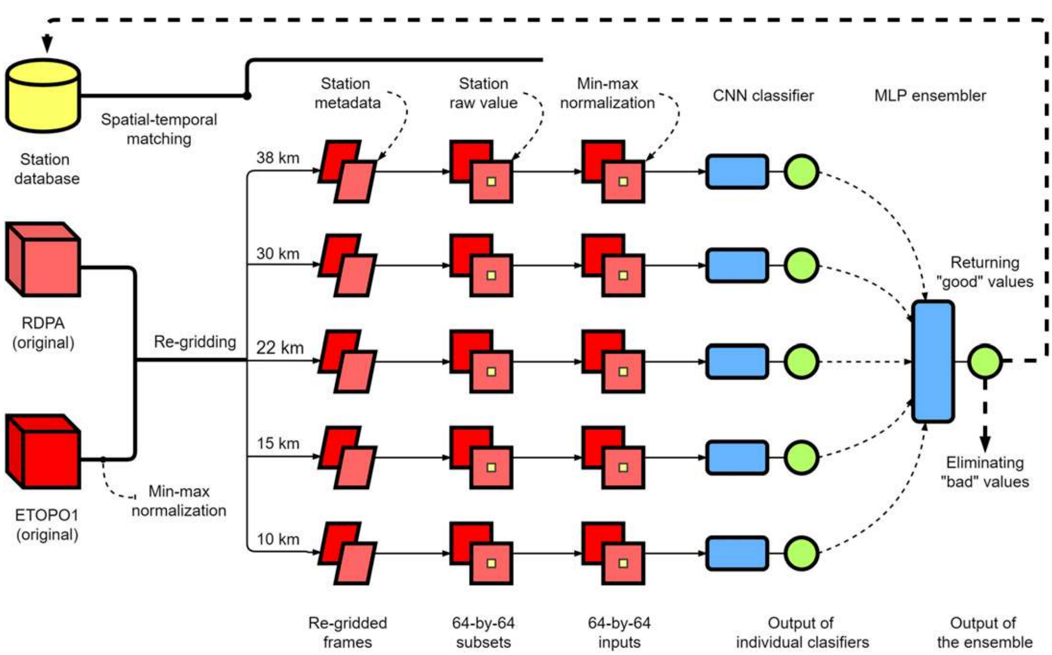

FIG. 4. The workflow of the QC system, where red and yellow objects indicate the data pipeline. Blue objects are the classifiers and multiscale classifier ensemble. Green circles are probabilistic outputs/QC flags.

1) MLPs (one for each grid spacing) are used as a non-CNN baseline. Each MLP classifier has 128 hidden layer nodes with tanh activation function and takes raw values and their nearest 64 regridded RDPA grid points as input.
2) Decision trees (one for each grid spacing) are used as another non-CNN baseline. Each decision tree classifier takes the same input as MLP baselines, and is trained independently in two stages. In stage 1, the trees are trained with Gini impurity and are allowed to grow to full size. In stage 2, the cost-complexity pruning algorithm is applied to remove the overfitted subtrees (Raileanu and Stoffel 2004; Breiman et al. 2017). The pruning factor is identified through a grid search, and is based on the validation set performance.
3) CNNs without elevation input (one for each grid spacing) are used as the CNN baseline. These CNN classifiers have the same architecture as the main classifiers in Fig. 2, but are configured without regridded elevation inputs.

The MLP and decision tree baselines are external; they were proposed by existing research, and were recognized as effective means for QC'ing gauge observations (Sciuto et al. 2009; Martinaitis et al. 2015; Qi et al. 2016), weather radar reflectivity (Lakshmanan et al. 2007), and radar precipitation (Lakshmanan et al. 2014). For avoiding the shift-of-region and -sample bias, external baselines are not directly ported from their original research, but rather, customized based on the data and learning task of this research. For the MLP baseline, we implemented the network architecture, activations, and training procedures of Lakshmanan et al. (2014), but assigned more hidden nodes for handling gridpoint-wise inputs. For the decision tree baseline, we replaced the knowledge-based tree split in Qi et al. (2016) with likelihood-based split, so the decision trees can be adapted to the BC Hydro (BCH) quality labels.

To our knowledge, no previous research has experimented with CNN-based precipitation QC. Thus, the CNN baseline of this research is internal. By comparing the CNN baseline with two external baselines, advantages of CNNs on incorporating gridded precipitation patterns around a station can be evaluated. Further, by comparing the main classifiers with the CNN baseline, the importance of incorporating gridded elevation can be identified.

e. Data preprocessing

1) Gauge observations

We select gauge observations from 80 BC Hydro stations from 0000 PST 1 January 2016 to 0000 PST 1 January 2018, and convert the raw and human QC'd gauge observations (where both were available) to precipitation rates (mm s^{-1}) by calculating the height and time difference from the previous observation. Missing values and negative precipitation rates are discarded.

The selected precipitation rates are resampled to every 30 min by linear interpolation. Each resampled value represents the average precipitation rate for the preceding 30 min. The goal of resampling is to prevent the QC system from overfitting specific combinations of stations and their observation intervals. If a precipitation rate with a different interval (e.g., hourly or 6 hourly) is desired by an end user, the QC'd 30-min rate(s) and quality flag(s) can be merged to the desired interval in a subsequent operational step.

We assign quality labels to the resampled raw precipitation rates (hereafter "raw values") by their additive difference from the resampled, human QC'd precipitation rates (hereafter "QC'd values"). If the difference between raw values and QC'd values was larger than 1/7200 mm h^{-1} (0.5 mm s^{-1}), that indicates the human QC process classified the raw value as bad (and thus changed it), and the value is labeled as "bad." Otherwise, a "good" quality flag will be assigned. We chose 1/7200 mm h^{-1} as the threshold value because the smallest possible difference that the lowest temporal resolution gauge data can report is 1 mm $(2\,h)^{-1}$, which converts to 1/7200 mm h^{-1}.

After preprocessing, 2 429 047 raw and QC'd value pairs are preserved; 1 972 840 (81.2%) samples have a raw value of zero and 456 207 (18.8%) are nonzero. We found 1 968 095 (99.8%) of the zero raw values have corresponding zero QC'd values, which means raw values of zero are almost surely good quality with no QC process needed. For nonzero raw values, 129 269 (28.3%) of them have bad-quality flags, so nonzero raw values need to be QC'd. Ignoring zero raw values also has the benefit of reducing the redundancy and skewness of samples.

Although the selected 80 BC Hydro stations are arranged within the same observation network, their type of instruments, observation frequency, and the number of nonzero raw values all vary. So their number of preserved samples after preprocessing varies. By watershed regions in the domain, the ratios of south coast, southern interior, and northeast BC station sample sizes are roughly 1:1.5:0.65, respectively (Fig. 1).

2) RDPA and ETOPO1

We regrid the RDPA and ETOPO1 datasets to regular latitude–longitude frames with roughly 38-, 30-, 22-, 15- and 10-km grid spacings. RDPA is also converted from 6-h accumulated precipitation (in mm) to precipitation rate (in mm s^{-1}) to match station value units.

3) Data matching, standardization, and separation

We pair the preprocessed observations and regridded RDPA/ETOPO1 spatially by searching the nearest regridded grid point for each station (hereafter "station grid point"). The regridded RDPA and ETOPO1 are cropped into 64×64 subsets centered on the station grid point. The 2×2 regridded RDPA values at the center of the cropping (i.e., the 32nd and 33rd grid points, where the 32nd grid point is the station grid point) are replaced by the raw observation value. The resulting 64×64 RDPA/raw-value croppings, along with the paired ETOPO1 croppings, form the CNN inputs (see Fig. 2b).

For temporal matching, each preprocessed RDPA frame represents the mean precipitation rate for the previous 6 h, whereas each resampled raw value represents the mean precipitation rate for the previous 30 min; the raw values and QC flags are matched with the RDPA time window that they fall within. Perfect temporal matching between RDPA and

TABLE 2. Metrics derived from confusion matrix elements and their meanings in this QC task.

Name and acronym	Definition	Explanation
True positives (TP)	—	Number of correctly classified bad observations
True negatives (TN)	—	Number of correctly classified good observations
False positives (FP)	—	Number of misclassified good observations (as bad), aka type I error
False negatives (FN)	—	Number of misclassified bad observations (as good), aka type II error
Condition positive (P)	TP + FN	Number of bad observations
Condition negative (N)	TN + FP	Number of good observations
True positive rate (TPR)	TP/(TP + FN)	Correctly classified bad observations relative to the real bad observations, aka sensitivity
True negative rate (TNR)	TN/(TN + FP)	Correctly classified good observations relative to the real good observations, aka specificity
False positive rate (FPR)	FP/(TN + FP)	Misclassified good observations relative to the real good observations
False negative rate (FNR)	FN/(TP + FN)	Misclassified bad observations relative to the real bad observations

observations is not needed because we are not performing point-to-point comparisons (see section 3a), and is impossible because of their frequency difference.

All datasets are standardized through minimum-maximum normalization. The precipitation input croppings are normalized independently to avoid the strong fluctuations of scales across dry and rainy seasons.

We use 2016 data for training; and data in 2017 within 15-day continuous periods starting at a random day of February, April, June, October for validation; and the rest of the 2017 data for testing. Training and validation data are split into balanced batches with each batch containing 100 bad raw value samples and 100 good raw value samples (i.e., a balanced batch size of 200). Testing data are grouped separately for evaluations. They contain 6700 bad and 24 060 good raw value samples, respectively. Note that missing RDPA data and the rounding of a fixed batch size will discard a small part of the preprocessed data.

4. Results

a. Classification verification metrics

We assign the ''good'' quality for a given observation as the true null hypothesis, or the ''negative class,'' because the majority of observations are of good quality; vice versa for ''bad'' quality and the ''positive class.''

We do not use regular categorical weather forecast verification metrics because many of them are positively oriented, which ignores the importance of accepting/rejecting the true null hypothesis. Instead, we derive QC metrics from confusion matrix elements (e.g., Wilks 2011) to verify QC classification results (Table 2). We also provide the receiver operating characteristic (ROC) curve and area under curve (AUC) for measuring the general classification performance.

If the QC classification is not well performed, we prefer to minimize type II errors [false negatives (FN)] more than type I errors [false positives (FP)] because type II errors introduce bad-quality observations into the QC'd dataset, and can cause larger impacts in operations downstream of the QC process.

The evaluation is based on a balanced subset of 13 400 samples randomly drawn from the testing set. We apply a unified 0.5 threshold for converting classification probabilities into binary labels, i.e., assigning positive class for output probabilities greater than or equal to 0.5. The choice of a 0.5 threshold provides a fair comparison between the main classifiers and baselines on a balanced testing set. The adjustment of thresholds for skewed data distributions are addressed in sections 4d and 6b.

b. General classification performance

The main classifiers outperform the CNN baseline, which in turn outperforms the decision tree and MLP baselines. The performance gain from decision tree/MLP to CNN baselines across all grid spacings, as indicated by lower false positive rate (FPR) and false negative rate (FNR) (cf. Figs. 5a–c), demonstrates the ability of CNN-based classifiers to extract effective representations from gridded precipitation inputs. The MLP baseline has the poorest performance, overperformed by decision trees that showed lower FNR and higher AUC (cf. Figs. 5a,b). A probable explanation is that MLPs are more affected by the training set overfitting, whereas the decision trees are pruned to down-weight input features with a high variance. Besides the good performance of complicated CNNs, we think decision-tree-based QC is also a valuable approach for its simplicity, and is a useful benchmark for classification-based QC comparison.

The performance gain of the main classifiers over the CNN baseline, due to the addition of gridded elevation inputs in the former, shows the ability of CNNs to utilize the provided elevation input (Figs. 5b,c). Performance gains for the main classifiers over the CNN baselines are found across all input grid spacings, with 38-km grid-spacing classifiers seeing the largest gain on true positive rate (TPR) (from 0.807 to 0.873), and 15-km grid-spacing classifiers showing the largest gain on true negative rate (TNR) (from 0.709 to 0.788).

For CNN baselines, 15- and 10-km (hereafter ''fine grid spacings'') classifiers and 38-, 30-, and 22-km (hereafter ''coarse grid spacings'') classifiers show clear differences; coarse grid spacings produce better (lower) FPR errors whereas fine grid spacings produce better (lower) FNR errors (Fig. 5b). This phenomenon is less prevalent in the main classifiers, indicating that by incorporating elevation inputs, which can represent

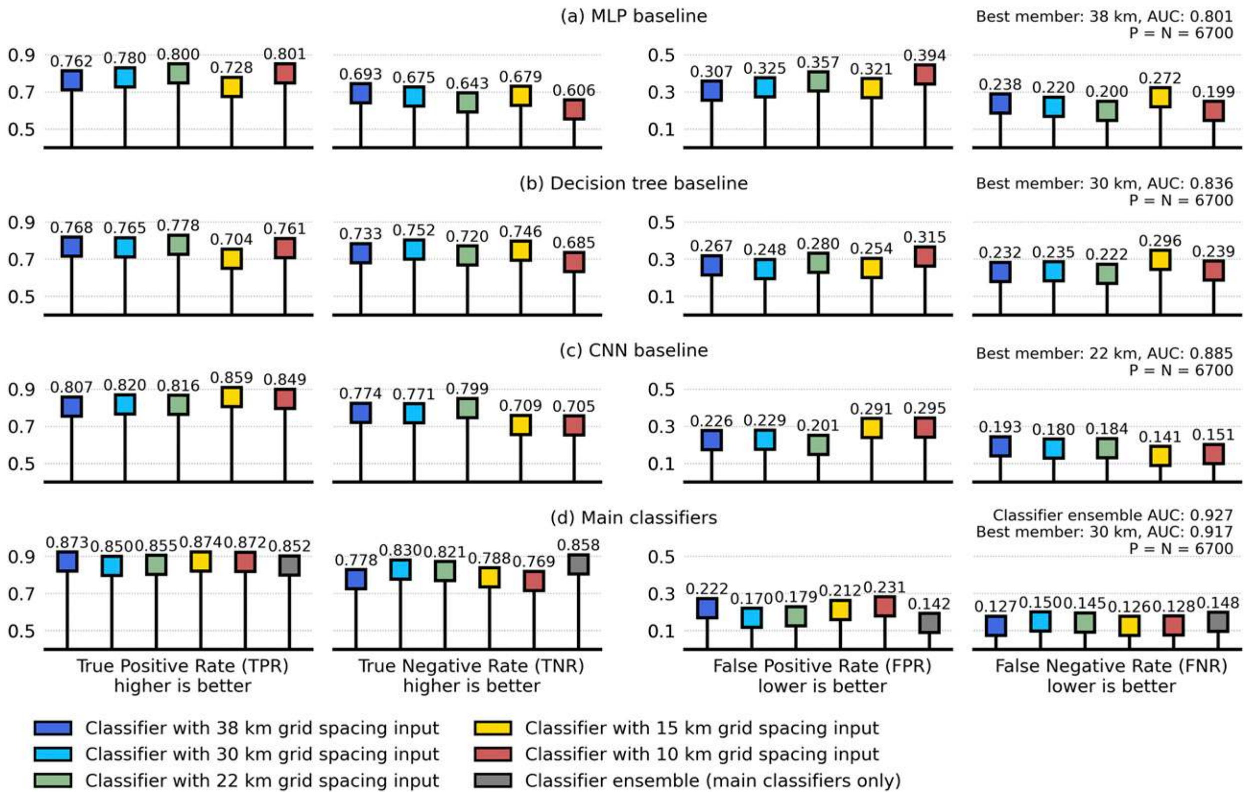

FIG. 5. Evaluation metrics (along bottom x axis) for (a) MLP baseline, (b) decision tree baseline, (c) CNN baseline, and (d) main classifiers. Text in the top right of all panels shows the AUC of the best single classifier member and (d) also includes the AUC for main classifier ensemble.

scale-sensitive precipitation–orography relationships, the impact of grid spacing is reduced.

The main classifier ensemble has the most balanced classification metrics with the lowest FNR; this is preferred in this QC problem because it introduces fewer bad values into the QC'd outputs.

We applied bootstrap aggregation (Breiman 1996) with 200 iterations to further evaluate the QC classification performance. For each iteration, a new testing set is formed with 13 400 samples. ROC and AUC are calculated during the bootstrap aggregation along with histograms (Fig. 6). The bootstrap aggregation (also known as ''bagging'') is performed by randomly sampling, and selecting the testing set, with replacement. Metrics are calculated on each sampling iteration independently. By measuring the variation of bootstrapped metrics, one can identify which classifier is most robust against testing set perturbations (a desired trait).

The results from bootstrapped AUCs are consistent with those from Fig. 5. The CNN baselines outperform the decision tree and MLP baselines, where the lowest bootstrapped AUC of the former are larger (better) than the highest bootstrapped AUC of the latter (cf. Figs. 6b–d). The worst performing main classifier also has its mean bootstrapped AUCs higher than the highest performing CNN baseline classifier (cf. Figs. 6c,d). Last, the bootstrapped AUCs of the main classifier ensemble are higher than the AUCs of any other single classifier member, confirming the performance gain of ensemble learning.

For both the main and baseline classifiers, better (higher) AUCs are found for coarse grid spacing members. The 30-km grid spacing works the best for the main classifier, and 38- and 22-km grid spacings work best for the MLP and CNN baselines. The 10-km grid spacing leads to the worst bootstrapped AUCs for all three classifier types (Figs. 6b–d).

Based on Fig. 6, the MLP baseline classifiers are the least robust, followed by the CNN baseline classifiers. Main classifiers have the lowest standard deviation, and so are the most robust classifiers.

c. *Classification performance by region and season*

The sample pool of this research has unequal numbers of stations within the three geographical regions (Fig. 1a), so it is important to examine the performance of main classifiers on a regional basis (Fig. 7).

The main classifiers behave differently across regions, with FNR larger than FPR for south coast stations, and the opposite for southern interior and northeast BC stations. The main classifier ensemble produces a relatively high AUC for the south coast and southern interior stations, indicating generally good classification performance in these two regions. For northeast BC stations, the main classifier ensemble AUC is lower, but given that most of the misclassification cases are

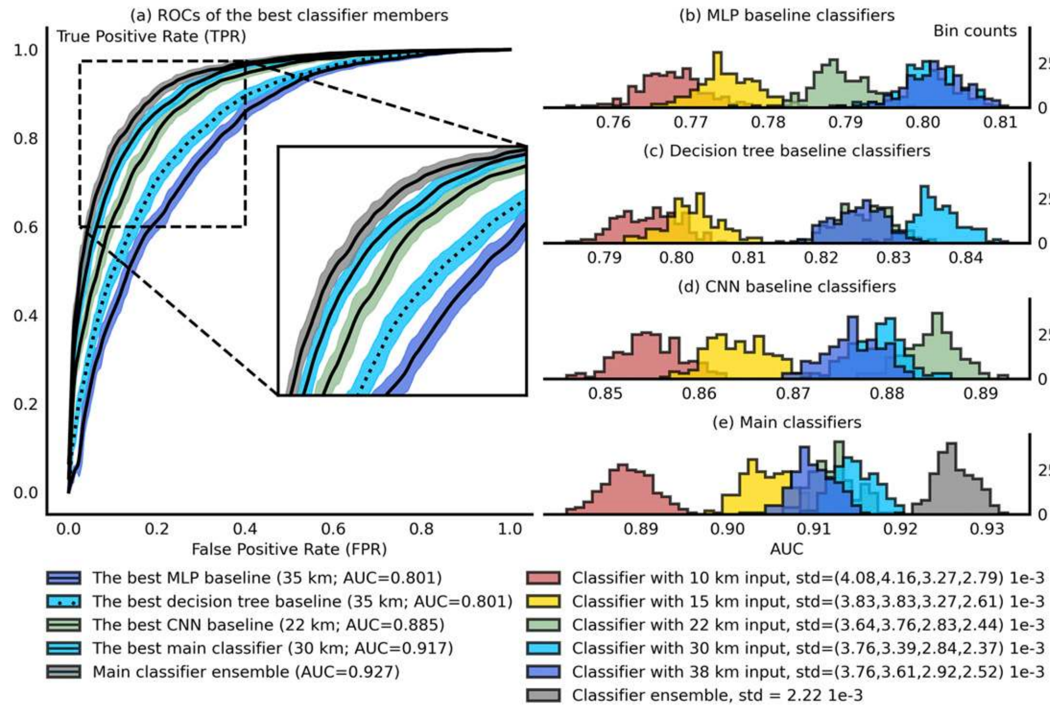

FIG. 6. (a) ROCs of best-performing grid spacing from each classifier configuration, and the main classifier ensemble. Shaded uncertainties are 3 times the standard deviations (std) of true positives during the bootstrap aggregation. (b)–(e) Histograms of AUCs from bootstrap aggregation for each classifier member and classifier configuration. The standard deviations of AUCs are listed in the legend at the bottom right with numbers representing classifiers in (b)–(e).

type I errors, the QC performance in this region is still acceptable—a relatively greater number of good values would be thrown out, but the remaining data would still be of high quality.

The best performing main classifier member varies among different regions. The 22-km grid-spacing classifier is the best member for the south coast; its AUC (0.861) is even higher than the classifier ensemble (0.860). The 30-km classifier is the best member for southern interior and northeast BC stations, its AUCs (0.828 and 0.793) are slightly lower than the classifier ensemble (0.840 and 0.802).

Note that northeast BC is the minority region of the sample pool (Fig. 1e). Thus, the low classification performances in this region could be attributed to their lower representativeness within the training data rather than the classifier itself.

The main classifier ensemble is also evaluated by season, with JJA/SON testing set classification results showing slightly better AUCs than those of DJF/MAM (Table 3). The DJF classification result shows relatively high type I error, similar to the evaluation of northeast BC stations—too many good-quality observations are misclassified as bad (high FPR), but the remaining data are of high quality (low FNR).

We further evaluate the main classifier ensemble for solid-precipitation-only observations in DJF. Given that BCH stations provide air temperature, but not humidity observations, solid precipitation is determined by a threshold of observed air temperature below −1.0°C (Table 3; both are resampled to every 30 min). This threshold is only used to select solid precipitation periods for evaluation purposes (i.e., not part of our method). Its value is relatively low compared with other studies (e.g., Motoyama 1990; Kienzle 2008; Liu et al. 2018) to ensure that virtually all of the selected observations are in the solid phase. The solid precipitation evaluation indicates an even higher type I error with low AUC (0.796), high FPR (0.319), and low FNR (0.087).

Two reasons that could explain the high type I error for the DJF testing set (and especially for solid precipitation) are 1) the RDPA data may underestimate the amount of solid precipitation (for details see section 2c), and 2) precipitation gauge inaccuracies are likely larger for solid precipitation. For example, wet snow can stick to the inside of the gauge orifice or form a cap over the top of the gauge, delaying the observed timing of solid precipitation events (Goodison et al. 1998). Both reason 1 and reason 2 could cause more frequent mismatches between the observed solid precipitation and the precipitation pattern indicated by the RDPA, encouraging the CNN classifiers to produce bad-quality flags.

Summarizing the general, region-specific, and season-specific evaluations, the main classifier ensemble performs the best. Its AUCs for the northeast BC stations, and DJF (especially for solid precipitation), are worse than other subsets of the data, but the cause of misclassification is type I error, which still ensures the quality of remaining data. Given that winter precipitation observation contains high uncertainty (Rasmussen et al. 2012),

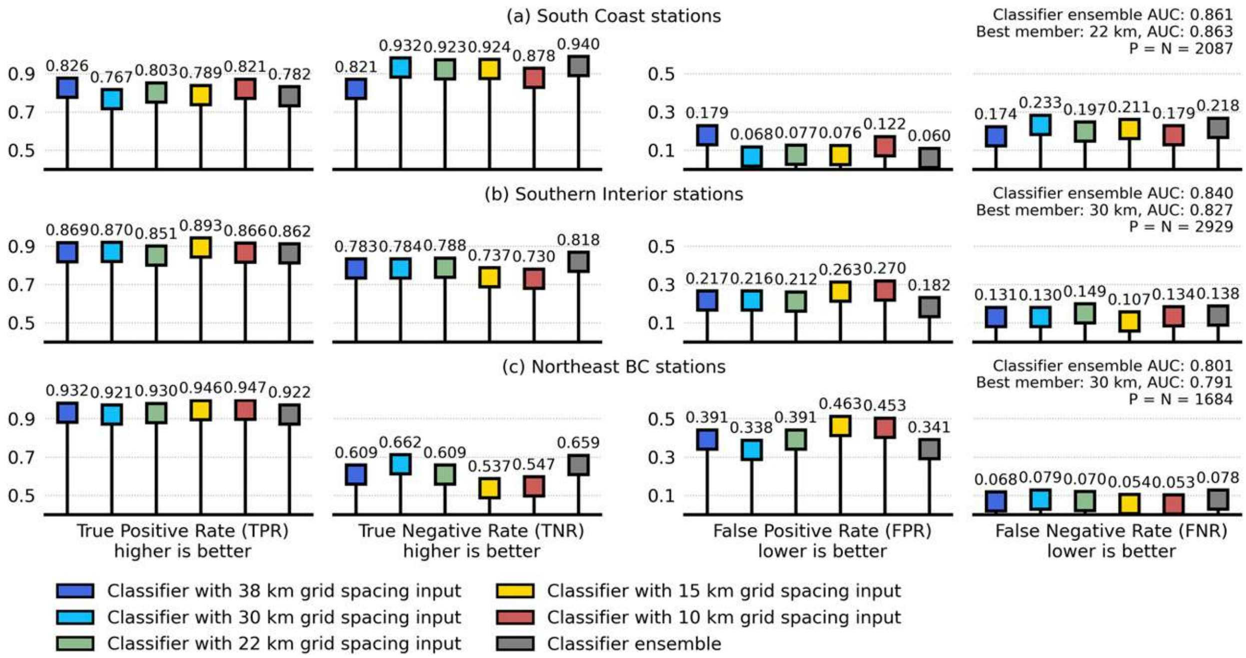

FIG. 7. Regional evaluation metrics for the main classifiers for (a) south coast stations, (b) southern interior stations, and (c) northeast BC stations. Text in the top right of each row shows the AUCs of the main classifier ensemble and best single classifier member, and the number of positive and negative samples that support this evaluation.

and is rejected very often in other automated QC research (e.g., Martinaitis et al. 2015), we feel the relatively high type I error of our method is an acceptable limitation.

d. Performance and adjustments on skewed data

Thus far we have evaluated our methods on balanced testing sets. In this section we explore adjusting the probabilistic threshold of our method on unbalanced data.

The illustration of classifier thresholding is based on synthesized "good station" and "bad station" cases. Good stations are positively skewed, with condition positive (P) smaller than condition negative (N; $P \ll N$); whereas the bad stations are negatively skewed, with $N \ll P$. We pick the first and last 25 stations in the rankings of N/P ratio for the above data synthesis. On average, good stations contain 95% good-quality raw values, whereas for bad stations this ratio is 39% (Fig. 8, right panel).

When a new station joins the observation network, no prior can be provided regarding its proportion of good and bad observations, one may choose 0.5 as the threshold. However, if this new station does not produce a comparable number of good and bad observations, the threshold of 0.5 can lead to suboptimal QC performance. If manual labels became available after the new station was established, then a thresholding step could be conducted. Figure 8 provides examples of this ROC-based thresholding that maximizes the difference of true positive (TP) and false positive (FP), with a grid search from 0.001 to 0.999. For the good station case, the optimized threshold is lower than 0.5, which identifies more bad observations by eliminating slightly more good observations, vice versa for the "bad station" case.

The QC performance is slightly worse for the bad stations, with a lower AUC (0.805, compared with 0.875 for the good stations (Fig. 8). However, given that for all 80 stations involved in this research, the overall percentage of good QC flags is 71.7% [see section 3e(1)], new stations are more likely to be similar to the "good station" case, where the QC classifiers and relatively low thresholds are expected to perform well.

TABLE 3. Evaluation metrics for the main classifier ensemble for different seasons in the testing set, and specifically for solid, winter precipitation. The threshold of the classifier is 0.5.

Season[a]	TP (TPR)	FP (FPR)	TN (TNR)	FN (FNR)	AUC	TP + FN	TN + FP
DJF	1512 (0.869)	286 (0.176)	1339 (0.824)	228 (0.131)	0.846	1740	1625
DJF, solid precipitation[b]	1075 (0.913)	326 (0.319)	695 (0.681)	102 (0.087)	0.797	1177	1021
MAM	1313 (0.848)	249 (0.152)	1389 (0.848)	235 (0.152)	0.848	1548	1638
JJA	1493 (0.853)	252 (0.145)	1484 (0.855)	257 (0.147)	0.854	1750	1736
SON	1421 (0.855)	253 (0.149)	1448 (0.851)	241 (0.145)	0.853	1662	1701

[a] Part of the February, April, June, and October days are not covered by the testing set (see section 3d).
[b] Solid precipitation is assumed to occur at air temperatures below −1.0°C.

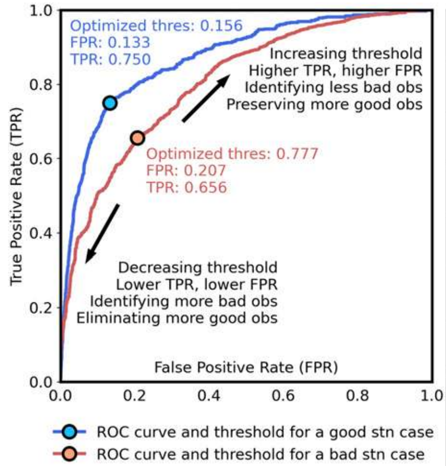

Metrics	A good stn case		A bad stn case	
Threshold	**0.156***	0.500	**0.777***	0.500
TP TPR	554 0.750	309 0.418	3201 0.656	4315 0.884
FP FPR	1850 0.133	444 0.032	657 0.207	1568 0.494
TN TNR	12100 0.867	13506 0.968	2514 0.793	1603 0.506
FN FNR	185 0.250	430 0.582	1681 0.344	567 0.116
AUC	0.875		0.805	
Number of bad obs (P)	739		4882	
Number of good obs (N)	13950		3171	

* : Optimized threshold based on the ROC curve (if the skewness case is known)

FIG. 8. (left) Two examples of the main classifier ensemble thresholding with ROC curves and (right) evaluation metrics before and after thresholding.

Note that thresholding is not part of the (probabilistic) classification, but a separated ''decision-making'' step. Thus, the training and evaluation of classifiers can still be based on balanced datasets. Meanwhile, by using information from the manual labels (see section 6d), the thresholding strategy can be tailored, for example, per season and per station.

e. Comparison with human QC

The human QC of BC Hydro station observations is based on 15-km RDPA precipitation maps and knowledge of orography—the same type of inputs as our method. This section compares the main CNN-based classifier QC to human QC by visual inspections of their agreements and disagreements. The example station selected here is a valley station located in the southern interior region.

Disagreements between CNN-based QC and human QC typically happen for low precipitation raw observation values that are outside of large-scale RDPA precipitation areas (FP), or high precipitation raw observation values that are within an RDPA low precipitation area (FN).

For the FP example (Fig. 9a, the purple mark), human QC marked it as good quality because its precipitation rate is lower than $0.2\,\mathrm{mm\,h^{-1}}$, roughly the same level as its corresponding 15-km RDPA gridpoint values (Fig. 9d). The CNN main classifier ensemble likely marked it as bad quality since in the coarser normalized precipitation fields (Fig. 9c), this nonzero precipitation value is far from a precipitation area.

For the FN example (Fig. 9a, the red mark), human QC corrected the raw value from $0.8\,\mathrm{mm\,h^{-1}}$ to zero because its surrounding 15-km RDPA grid points showed lower, near-zero precipitation rates. On the contrary, CNN likely marked it as good quality because this nonzero precipitation is within precipitation areas, close to and downstream of similarly high precipitation rates in the southwest BC (Fig. 9f).

Since human labels are not perfect in every single case, we cannot tell which QC method is correct for these two examples. We can, however, see from Fig. 7a that the CNN-based QC is making reasonable decisions for the majority of data points, focusing on proximity, magnitudes, and precipitation patterns.

5. Interpretation analysis

Based on the analysis of classification performance in section 4, two important findings remain unexplained: 1) The grid spacing of the original RDPA data is about 10 km, but the classifier that takes 10 km grid spacing input features showed the worst performance (Figs. 6b–d). Aggregated coarse input benefits discrimination for all classifier configurations including the two baselines and the main classifiers. 2) The main classifier ensemble is, in general, the best discriminator, but it is outperformed by the main classifier member with 22-km grid-spacing input for south coast stations.

For the first finding above, our hypothesis is that the RDPS forecast, which provides the background field of the RDPA, has lower skill for small-scale precipitation details. For the second finding, our hypothesis is that the 22-km classifier can extract a unique scale of precipitation pattern that is specific to the QC of south coast stations. These hypotheses are investigated via interpretation analyses of pretrained CNNs.

The evaluation tool we use in this section is the saliency map. When applied to CNNs, a saliency map visualizes the computed gradient of the class score with respect to a given input sample and a given hidden neuron (Simonyan and Zisserman 2015). By visualizing the class score gradients, the predictive importance of each hidden neuron for each input sample can be diagnosed. In this research, saliency maps give insights as to which part of the gridded precipitation and elevation fields attracts the CNNs' ''attention'' for decision-making. By investigating this information, process-based evaluation can be applied, which is expected to explain the two findings identified above.

For each main classifier, we compute its saliency maps from 1) the last hidden-layer neurons with positive weights, 2) the

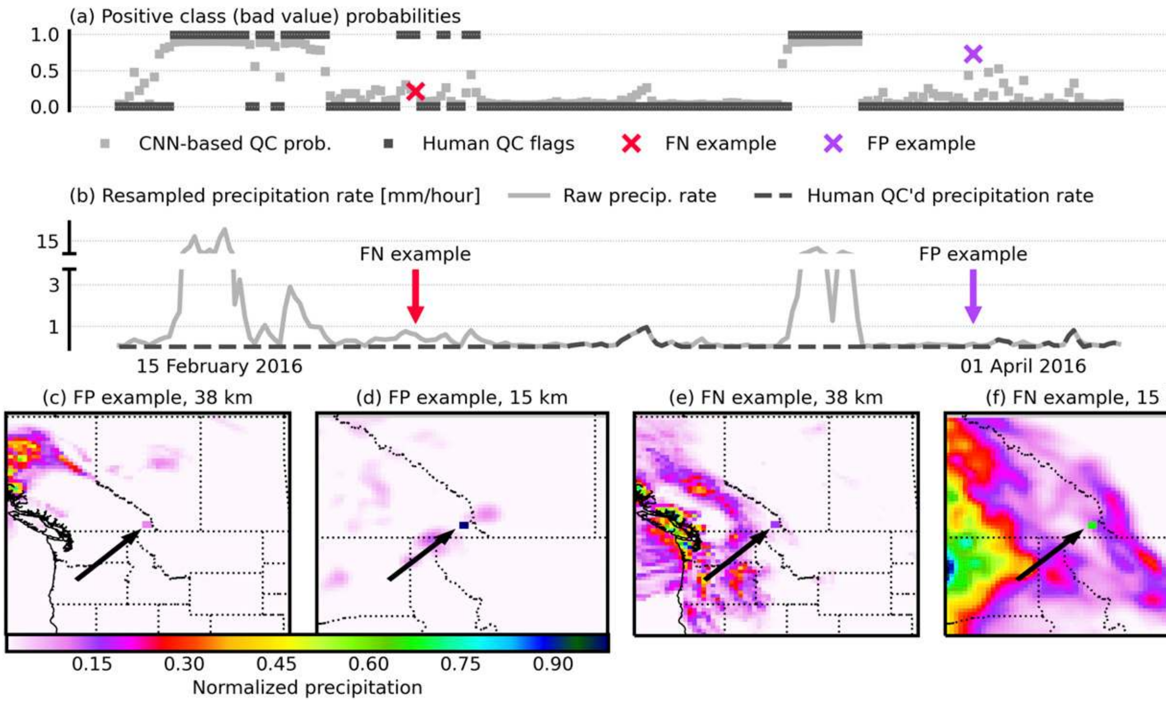

FIG. 9. Comparison of CNN-based QC and human QC for a southern interior station from 15 Feb to 1 Apr 2016. (a) Time series of bad-value probabilities estimated by the CNN classifier ensemble (gray) and human QC flags (black). (b) Raw (gray solid) and human-QC'd (black dashed) precipitation rates. Red and purple markings in (a) and (b) denote the same false negative (FN) and false positive (FP) examples in each plot, respectively. (c)–(f) RDPA precipitation field corresponding to each example; 38- and 15-km grid-spacing precipitation fields are shown for the two cases. Arrows point to the precipitation field grid box that has been replaced by raw station values.

top 200 true negative (TN; correctly classified negative class) training samples, and 3) the precipitation input channel. In total, this results in 80 000 saliency maps per classifier (400 neurons × 200 samples × 1 channel).

Many existing studies directly choose the saliency map computed from neurons with the highest weight or simply show some successful examples (e.g., Springenberg et al. 2015; Zeiler and Fergus 2014). However, the hidden neuron with the highest weights is not guaranteed to be the hidden neuron with the strongest discriminative abilities. In this research, we use the empirical orthogonal function (EOF) analysis to reduce the dimensionality of all 80 000 saliency maps by extracting the most representative spatial patterns and their corresponding coefficient series. EOF (also known as the principal component analysis) is an exploratory data analysis algorithm that reduces the dimensionality (and thus, the complexity) of data by extracting components of the data that explain the highest amount of variation (Wilks 2011).

EOF is performed on saliency maps subsets as grouped by classifier and region. Each of the three regions (Fig. 1) is represented by the station that appeared most frequently among all the selected neurons. This selection typically leads to 200–5000 saliency maps for each saliency map subset. We preserve only the first mode of the EOF, and its corresponding precipitation input precipitation field is calculated from the composite of the positive EOF coefficient series. After EOF-based dimensionality reduction, 15 compressed saliency fields (black contours, Fig. 10) and their corresponding composite of input feature fields (color shading, Fig. 10) are formed; together they illustrate the most representative pattern of the gradient class score for a given main classifier and region. For visualization purposes, saliency maps are filtered by Gaussian smoothers to remove the "checkerboard artifacts."

Input feature map grid points with positive saliency map values (gradient of class scores) indicate the discriminatory ability of a given neuron for the positive class, and vice versa. Here, since all the saliency maps are computed for TN samples, we will focus on the input precipitation field with negative saliency map values. Also, since we have compressed the saliency maps as EOF modes, the saliency map values here represent an abstract of all the selected neurons. In general, negative saliency map values are found around the location of the station. Since the raw station precipitation values are ensured to be nonzero, this means the positive precipitation values around the station benefits the discrimination of this raw value as the negative class (a good observation). Negative saliency map values are also found far removed from the station locations. These negative values contribute to the CNN's discrimination for good observations, and thus (based on the "opinions" of the CNNs) indicate the locations of the remote precipitation areas that are associated with precipitation at the station location and within the 6-h RDPA time window.

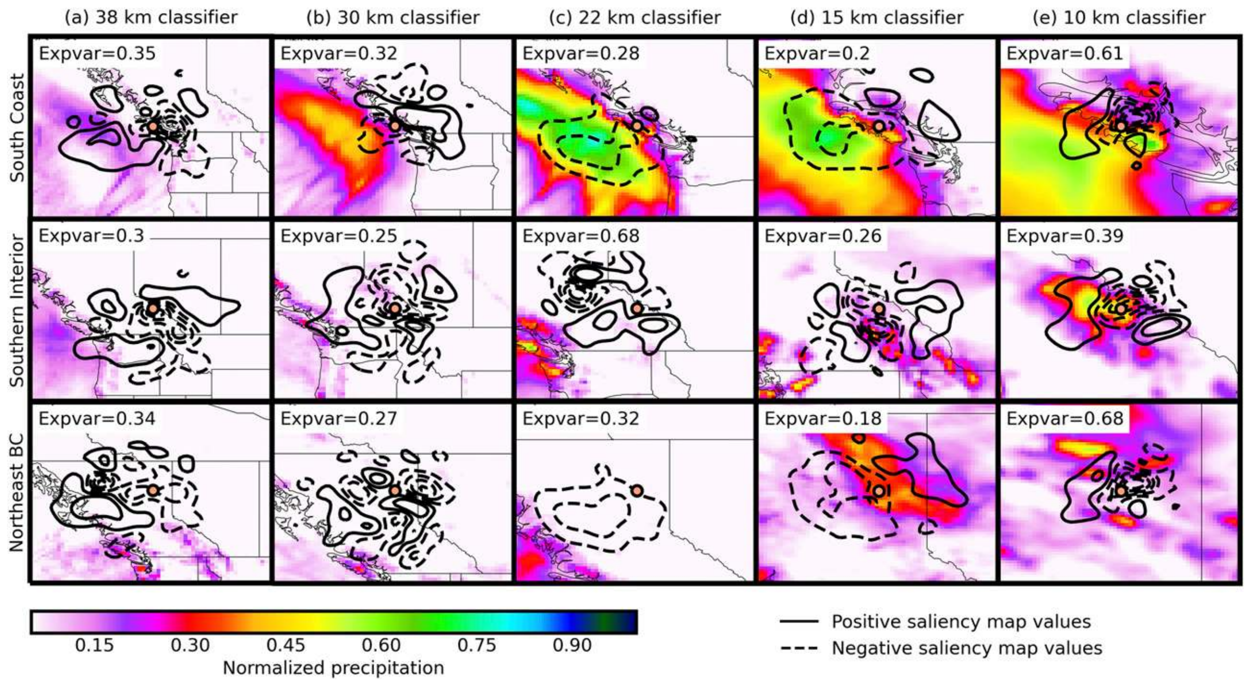

FIG. 10. Saliency maps for the five main classifiers for three stations (orange dots) that represent the three regions in this study. Black contours are the standardized and filtered first EOF mode of the gradient of class score. The explained variance of the EOF mode is shown in the top left of each panel. Color shading is the composite of normalized RDPA precipitation fields from the positive EOF coefficient series.

We now use the saliency maps (Fig. 10) to investigate the two unexplained findings above. For 1), we see that the 10-km classifier has the smallest, most concentrated area of negative saliency map values close to the location of stations (dashed contours, Fig. 9, right column). This means the 10-km classifier tends to focus on very localized precipitation patterns around the station, without considering larger-scale precipitation patterns. As was mentioned in section 2c, the gridded precipitation input (from the RDPA) is mainly populated by model forecast background fields around BC Hydro stations. These forecasted small-scale precipitation patterns are not guaranteed to be correct, and thus may have low predictive skill for QC, which would have negative impacts on classification. This likely explains why its performance is the worst among all main classifiers, lending support to our first hypothesis above.

For 2), the superior performance of the 22-km grid-spacing classifier for south coast stations, we see large negative saliency map values extending southwestward from the Vancouver Island station, which aligns well with the typical path and scale of an approaching midlatitude front (e.g., Neiman et al. 2008; Read 2015). Thus, this classifier is highly beneficial for discriminating nonzero raw values as the negative class (good observations). The 22-km grid-spacing classifier does not do equally well in the other two regions. For example, in northeast BC similar southwesterly patterns exist (Fig. 10c, third row), but since precipitation is fundamentally different (often approaching from the east), the success of this negative saliency pattern is not reproduced.

Other map properties lend additional insights concerning the success of coarser grid spacing classifiers. For example, these classifiers typically make larger and sometimes multidirectional negative saliency map values that connect the major precipitation areas and the station locations. The 38- and 30-km grid-spacing classifiers have negative saliency map values that extend both southwestward to northeastward, which explains their good performance in the southern interior and northeast BC (Figs. 7b,c). The saliency map values of the 22- and 15-km classifiers incorporate a larger number of grid points than coarser classifiers, which partially compensates for the smaller input domain of the finer grid spacing classifiers. The magnitudes of normalized precipitation increase with finer grid spacing, indicating that the contributing RDPA grids either have precipitation features that are more concentrated, well defined, and/or more consistently positioned (such that features are not averaged out). All of these could be properties of orographic precipitation resolved by finer-scale grids. The coarser grids feature weaker precipitation gradients, which could result from less concentrated or defined precipitation features, and/or less consistent positioning of those features (such that details are averaged out).

6. Discussion

a. *CNN-based QC compared to neighboring-station-based QC*

As explained in section 3, this research used gridded values around target stations to cross validate the quality of those stations' observations. This approach is similar to the neighboring station approach in that the grid points used here can be viewed as the "surrogate stations." Individual RDPA grid point values are not as reliable as good-quality station observations; however, collectively the 64×64 sized inputs provide useful information for cross validating the target station observations.

Compared to the classic neighboring station approach (e.g., Hubbard et al. 2005), the use of gridded data has advantages for QC'ing stations in complex terrain regions and/or regions where reference stations are sparse. We have shown that CNN-based classifiers can effectively use spatial patterns from both precipitation and elevation gridded inputs for station observation QC, and the classification result is largely improved over spatially agnostic models like MLP and decision trees. We think this finding further implies the potential of deep-learning-based QC as an alternative to other automated QC methods for handling more diverse input data forms.

b. Notes on data skewness

Our method was trained on a balanced dataset and based on the evaluations in section 4c, it performs well for positively skewed (more good observations than bad observations) stations. This guarantees the reliability of our method for most BC Hydro stations. For the uncommon "bad stations," where QC flags are negatively skewed, some solutions are available. For example, prior stand-alone checks, such as range checks, common bad value checks and rate of change checks can reduce the number of positive samples. Additionally, one could create a small human-QC'd validation dataset for the negatively skewed station, and tune QC classifiers on that dataset (e.g., Platt 1999; Niculescu-Mizil and Caruana 2005). This fine-tuning can be performed at either the ensemble level or the single classifier level.

Another problem typically associated with data skewness is the "precision-recall tradeoff"—the trade-off between maximizing TPR and TNR. As shown in Figs. 5 and 6, the main classifier ensemble is a balanced classifier—for a balanced testing set, it classifies good and bad observations equally well. In an operational setting with big data pools, higher TNR (lower type II error) could be more important. That is, users may prefer to lose (misclassify) some good observations to correctly eliminate more bad observations (minimize FNR), due to the larger downstream impacts of bad observations. This is an important point: a user can choose to improve the system's FNR by simply lowering the threshold of bad-observation probability (i.e., below 0.5).

c. Generalization and input data replacement

Our method requires gridded precipitation data as an input, and in this research, the RDPA is applied. Could one use other gridded precipitation data to replace the RDPA for other observation networks and outside of BC?

Based on the interpretation analysis in section 5, our method implicitly compares a gauge observational value with its surrounding precipitation patterns from a gridded analysis. Many successfully QC'd nonzero gauge observations are located either within or at the edge of a synoptic-scale precipitation pattern. This finding is identified for 38–15-km grid-spacing inputs and both coastal and interior watersheds—it is not specific to a certain grid spacing or geographical location. That said, if a gridded input other than the RDPA can roughly represent the spatial coverage of precipitation events, then we have no a priori reason to expect the performance would be downgraded. We think exploiting different gridded inputs as QC reference fields is a possible future research direction.

Further, as described in section 3a, the CNN-based QC is based on pattern-to-station rather than gridpoint-to-station comparisons, and thus, it has some robustness against the position errors of gridded precipitation data. For most of the BC Hydro watersheds in this research, the RDPA is mainly populated by the RDPS forecast model, with limited precipitation gauge calibrations. This deficiency impacted the CNN-base methods less than the other two external baselines. Thus, for generalizing CNN-based observation QC to a broader extent, one could either adapt the classifier configuration and data preprocessing of this research, or build new CNN classifiers from scratch. However, we do recommend a post hoc interpretation analysis, similar to our section 5, to ensure that the proposed CNNs are utilizing precipitation pattern information.

d. Learning from and collaborative improvement of the CNNs

Machine learning interpretation methods like the saliency maps employed herein give insights into the decision-making of the CNN-based QC model. These insights can, in turn, bring inspiration to human QC procedures. Based on the comparisons in section 4d and interpretations in section 5, the CNN values the distribution of precipitation patterns upstream of the station. This suggests that human QC should also focus more on cross validations using stations/data sources upstream of a target station, rather than simply looking at all nearby values. Based on the intercomparison of main classifier members, regridding precipitation data to coarser grid spacings may be another way to improve manual and/or automated QC workflows.

Human QC staff could also work collaboratively with the CNN-based QC. One possible configuration would be for the CNNs to perform the first round of QC to categorize high-confidence good and bad observations. The human QC staff would then perform a second round to categorize the observations that have less certain quality probabilities close to 0.5. The above combination reduces human workload and gives them more time to focus on the more important and difficult QC cases. Also, when the second round human QC is completed, the resulting QC labels can be used to further tune and improve the classification performance and thresholding of the CNN.

7. Conclusions

We proposed ResNet-like CNNs with multiscale classifier ensembles for the automated QC of a sparse precipitation observation network in complex terrain. The CNNs are trained with human QC'd labels through supervised learning and can classify raw observation values by taking regridded (coarsened) precipitation analyses (RDPA) and elevation (ETOPO1) as inputs. Based on classification metrics, our

CNN-based QC separates ''good'' and ''bad'' observations well, with an overall area under curve (AUC) of 0.927 and type I/type II error lower than 15%.

Our approach has minor limitations when handling 1) solid precipitation in DJF and 2) very problematic stations (stations where bad observations largely outnumber the good). Solid precipitation QC tends to eliminate somewhat more good observations, but the preserved values are still of good quality. The issue with problematic stations could be overcome by fine-tuning the model for these types of stations using a smaller human-labeled dataset. Aside from these limitations, our CNN-based QC is effective and could be generalized to other observation networks for a variety of use cases.

To our knowledge, this is the first study that implements CNN classifiers for precipitation observation quality control, and explains why CNNs can make better QC decisions. We found that coarser grid spacing (i.e., 38-, 30-, 22-km) inputs yielded better CNN performance, and the CNNs can detect abnormal nonzero raw observational values by taking into account the station locations relative to other neighboring and upstream precipitation patterns. This saliency information learned from CNNs could also help inform human QC operations.

Acknowledgments. This research is jointly funded by a Four Year Doctoral Fellowship (4YF) program of the University of British Columbia, and the Canadian Natural Science and Engineering Research Council (NSERC). We thank BC Hydro, and the Environment and Climate Change Canada (ECCC) for providing the data. We also thank the Casper cluster [Computational and Information Systems Laboratory (CISL); CISL 2020], the National Center for Atmospheric Research (NCAR), and their Advanced Study Program (ASP) for supporting this research. NCAR is operated by the University Corporation for Atmospheric Research (UCAR) and is sponsored by the National Science Foundation. Additional support was provided by MITACS and BC Hydro. We also thank the three anonymous reviewers for their comments and suggestions which improved this manuscript.

REFERENCES

Adam, J. C., and D. P. Lettenmaier, 2003: Adjustment of global gridded precipitation for systematic bias: Global gridded precipitation. *J. Geophys. Res.*, **108**, 4257, https://doi.org/10.1029/2002JD002499.

Adler, R. F., and Coauthors, 2003: The version-2 Global Precipitation Climatology Project (GPCP) monthly precipitation analysis (1979–present). *J. Hydrometeor.*, **4**, 1147–1167, https://doi.org/10.1175/1525-7541(2003)004<1147:TVGPCP>2.0.CO;2.

Amante, C., and B. Eakins, 2009: ETOPO1 Arc-Minute Global Relief Model: Procedures, data sources and analysis. National Geophysical Data Center Marine Geology and Geophysics Division Rep., 25 pp.

Banta, R. M., and Coauthors, 2013: Observational techniques: Sampling the mountain atmosphere. *Mountain Weather Research and Forecasting: Recent Progress and Current Challenges*, F. K. Chow, S. F. De Wekker, and B. J. Snyder, Eds., Springer Atmospheric Sciences, 409–530, https://doi.org/10.1007/978-94-007-4098-3_8.

BC Hydro, 2020: Generation System: An efficient, low cost electricity system for B.C. Accessed 13 May 2020, https://www.bchydro.com/energy-in-bc/operations/generation.html.

Breiman, L., 1996: Bagging predictors. *Mach. Learn.*, **24**, 123–140, https://doi.org/10.1007/BF00058655.

——, J. H. Friedman, R. A. Olshen, and C. J. Stone, 2017: *Classification and Regression Trees*. 1st ed. Routledge, 368 pp., https://doi.org/10.1201/9781315139470.

Canadian Centre for Climate Services, 2019: Technical documentation: Regional Deterministic Precipitation Analysis (RDPA). Government of Canada, https://www.canada.ca/en/environment-climate-change/services/climate-change/canadian-centre-climate-services/display-download/technical-documentation-regional-precipitation-analysis.html.

Carrera, M. L., S. Bélair, V. Fortin, B. Bilodeau, D. Charpentier, and I. Doré, 2010: Evaluation of snowpack simulations over the Canadian Rockies with an experimental hydrometeorological modeling system. *J. Hydrometeor.*, **11**, 1123–1140, https://doi.org/10.1175/2010JHM1274.1.

Chilton, R. R. H., 1981: A summary of climatic regimes of British Columbia. Ministry of Environment Assessment and Planning Division Rep., 44 pp.

CISL, 2020: Cheyenne: HPE/SGI ICE XA system (NCAR Community Computing). National Center for Atmospheric Research, https://doi.org/10.5065/d6rx99hx.

Eischeid, J. K., C. B. Baker, T. R. Karl, and H. F. Diaz, 1995: The quality control of long-term climatological data using objective data analysis. *J. Appl. Meteor.*, **34**, 2787–2795, https://doi.org/10.1175/1520-0450(1995)034<2787:TQCOLT>2.0.CO;2.

——, P. A. Pasteris, H. F. Diaz, M. S. Plantico, and N. J. Lott, 2000: Creating a serially complete, national daily time series of temperature and precipitation for the western United States. *J. Appl. Meteor.*, **39**, 1580–1591, https://doi.org/10.1175/1520-0450(2000)039<1580:CASCND>2.0.CO;2.

Fortin, V., G. Roy, N. Donaldson, and A. Mahidjiba, 2015: Assimilation of radar quantitative precipitation estimations in the Canadian Precipitation Analysis (CaPA). *J. Hydrol.*, **531**, 296–307, https://doi.org/10.1016/j.jhydrol.2015.08.003.

——, ——, T. Stadnyk, K. Koenig, N. Gasset, and A. Mahidjiba, 2018: Ten years of science based on the Canadian Precipitation Analysis: A CaPA system overview and literature review. *Atmos.–Ocean*, **56**, 178–196, https://doi.org/10.1080/07055900.2018.1474728.

Goodfellow, I., Y. Bengio, and A. Courville, 2016: *Deep Learning: Adaptive Computation and Machine Learning*. MIT Press, 775 pp.

Goodison, B. E., P. Y. T. Louie, and D. Yang, 1998: WMO solid precipitation measurement intercomparison—Final report. WMO Rep. 67, 318 pp., https://www.wmo.int/pages/prog/www/IMOP/publications/IOM-67-solid-precip/WMOtd872.pdf.

Groisman, P. Ya., and D. R. Legates, 1994: The accuracy of United States precipitation data. *Bull. Amer. Meteor. Soc.*, **75**, 215–228, https://doi.org/10.1175/1520-0477(1994)075<0215:TAOUSP>2.0.CO;2.

Gu, J., and Coauthors, 2018: Recent advances in convolutional neural networks. *Pattern Recognit.*, **77**, 354–377, https://doi.org/10.1016/j.patcog.2017.10.013.

He, K., X. Zhang, S. Ren, and J. Sun, 2015a: Deep residual learning for image recognition. arXiv, http://arxiv.org/abs/1512.03385.

——, ——, ——, and ——, 2015b: Delving deep into rectifiers: surpassing human-level performance on ImageNet classification. *2015 IEEE Int. Conf. on Computer Vision*, IEEE, Santiago, Chile, 1026–1034, https://doi.org/10.1109/ICCV.2015.123.

Hubbard, K. G., S. Goddard, W. D. Sorensen, N. Wells, and T. T. Osugi, 2005: Performance of quality assurance procedures for an applied climate information system. *J. Atmos. Oceanic Technol.*, **22**, 105–112, https://doi.org/10.1175/JTECH-1657.1.

Ioffe, S., and C. Szegedy, 2015: Batch normalization: Accelerating deep network training by reducing internal covariate shift. arXiv, http://arxiv.org/abs/1502.03167.

Jiang, S., M. Lian, C. Lu, Q. Gu, S. Ruan, and X. Xie, 2018: Ensemble prediction algorithm of anomaly monitoring based on big data analysis platform of open-pit mine slope. *Complexity*, **2018**, 1048756, https://doi.org/10.1155/2018/1048756.

Jørgensen, H. K., S. Rosenørn, H. Madsen, and P. S. Mikkelsen, 1998: Quality control of rain data used for urban runoff systems. *Water Sci. Technol.*, **37**, 113–120, https://doi.org/10.2166/wst.1998.0448.

Kienzle, S. W., 2008: A new temperature based method to separate rain and snow. *Hydrol. Processes*, **22**, 5067–5085, https://doi.org/10.1002/hyp.7131.

Kingma, D. P., and J. Ba, 2017: Adam: A method for stochastic optimization. arXiv, http://arxiv.org/abs/1412.6980.

Lakshmanan, V., A. Fritz, T. Smith, K. Hondl, and G. Stumpf, 2007: An automated technique to quality control radar reflectivity data. *J. Appl. Meteor. Climatol.*, **46**, 288–305, https://doi.org/10.1175/JAM2460.1.

——, C. Karstens, J. Krause, and L. Tang, 2014: Quality control of weather radar data using polarimetric variables. *J. Atmos. Oceanic Technol.*, **31**, 1234–1249, https://doi.org/10.1175/JTECH-D-13-00073.1.

Lespinas, F., V. Fortin, G. Roy, P. Rasmussen, and T. Stadnyk, 2015: Performance evaluation of the Canadian Precipitation Analysis (CaPA). *J. Hydrometeor.*, **16**, 2045–2064, https://doi.org/10.1175/JHM-D-14-0191.1.

Liu, Y., and Coauthors, 2016: Application of deep convolutional neural networks for detecting extreme weather in climate datasets. arXiv, http://arxiv.org/abs/1605.01156.

——, G. Ren, X. Sun, and X. Li, 2018: A new method to separate precipitation phases. *Hydrol. Earth Syst. Sci. Discuss.*, https://doi.org/10.5194/hess-2018-307.

Mahfouf, J.-F., B. Brasnett, and S. Gagnon, 2007: A Canadian Precipitation Analysis (CaPA) project: Description and preliminary results. *Atmos.–Ocean*, **45**, 1–17, https://doi.org/10.3137/ao.v450101.

Martinaitis, S. M., S. B. Cocks, Y. Qi, B. T. Kaney, J. Zhang, and K. Howard, 2015: Understanding winter precipitation impacts on automated gauge observations within a real-time system. *J. Hydrometeor.*, **16**, 2345–2363, https://doi.org/10.1175/JHM-D-15-0020.1.

Maul-Kötter, B., and T. Einfalt, 1998: Correction and preparation of continuously measured raingauge data: A standard method in North Rhine-Westphalia. *Water Sci. Technol.*, **37**, 155–162, https://doi.org/10.2166/wst.1998.0458.

Meek, D., and J. Hatfield, 1994: Data quality checking for single station meteorological databases. *Agric. For. Meteor.*, **69**, 85–109, https://doi.org/10.1016/0168-1923(94)90083-3.

Motoyama, H., 1990: Simulation of seasonal snowcover based on air temperature and precipitation. *J. Appl. Meteor.*, **29**, 1104–1110, https://doi.org/10.1175/1520-0450(1990)029<1104:SOSSBO>2.0.CO;2.

Mourad, M., and J.-L. Bertrand-Krajewski, 2002: A method for automatic validation of long time series of data in urban hydrology. *Water Sci. Technol.*, **45**, 263–270, https://doi.org/10.2166/wst.2002.0601.

Nearing, M. A., and Coauthors, 2005: Modeling response of soil erosion and runoff to changes in precipitation and cover. *Catena*, **61**, 131–154, https://doi.org/10.1016/j.catena.2005.03.007.

Neiman, P. J., F. M. Ralph, G. A. Wick, J. D. Lundquist, and M. D. Dettinger, 2008: Meteorological characteristics and overland precipitation impacts of atmospheric rivers affecting the west coast of North America based on eight years of SSM/I satellite observations. *J. Hydrometeor.*, **9**, 22–47, https://doi.org/10.1175/2007JHM855.1.

Niculescu-Mizil, A., and R. Caruana, 2005: Predicting good probabilities with supervised learning. *Proc. 22nd Int. Conf. on Machine Learning*, Bonn, Germany, ACM, 625–632, https://doi.org/10.1145/1102351.1102430.

Null, S. E., J. H. Viers, and J. F. Mount, 2010: Hydrologic response and watershed sensitivity to climate warming in California's Sierra Nevada. *PLOS ONE*, **5**, e9932, https://doi.org/10.1371/journal.pone.0009932.

Odon, P., G. West, and R. Stull, 2018: Evaluation of reanalyses over British Columbia. Part I: Daily and extreme 2-m temperature. *J. Appl. Meteor. Climatol.*, **57**, 2091–2112, https://doi.org/10.1175/JAMC-D-18-0058.1.

Piatyszek, E., P. Voignier, and D. Graillot, 2000: Fault detection on a sewer network by a combination of a Kalman filter and a binary sequential probability ratio test. *J. Hydrol.*, **230**, 258–268, https://doi.org/10.1016/S0022-1694(00)00213-4.

Platt, J. C., 1999: Probabilistic outputs for support vector machines and comparisons to regularized likelihood methods. *Advances in Large Margin Classifiers*, MIT Press, 61–74.

Qi, Y., S. Martinaitis, J. Zhang, and S. Cocks, 2016: A real-time automated quality control of hourly rain gauge data based on multiple sensors in MRMS system. *J. Hydrometeor.*, **17**, 1675–1691, https://doi.org/10.1175/JHM-D-15-0188.1.

Raileanu, L. E., and K. Stoffel, 2004: Theoretical comparison between the Gini index and information gain criteria. *Ann. Math. Artif. Intell.*, **41**, 77–93, https://doi.org/10.1023/B:AMAI.0000018580.96245.c6.

Rasmussen, R., and Coauthors, 2012: How well are we measuring snow: The NOAA/FAA/NCAR winter precipitation test bed. *Bull. Amer. Meteor. Soc.*, **93**, 811–829, https://doi.org/10.1175/BAMS-D-11-00052.1.

Read, W. A., 2015: The climatology and meteorology of windstorms that affect southwest British Columbia, Canada, and associated tree-related damage to the power distribution grid. Ph.D. thesis, University of British Columbia, 383 pp., https://doi.org/10.14288/1.0166485.

Schneider, U., A. Becker, P. Finger, A. Meyer-Christoffer, M. Ziese, and B. Rudolf, 2014: GPCC's new land surface precipitation climatology based on quality-controlled in situ data and its role in quantifying the global water cycle. *Theor. Appl. Climatol.*, **115**, 15–40, https://doi.org/10.1007/s00704-013-0860-x.

Sciuto, G., B. Bonaccorso, A. Cancelliere, and G. Rossi, 2009: Quality control of daily rainfall data with neural networks. *J. Hydrol.*, **364**, 13–22, https://doi.org/10.1016/j.jhydrol.2008.10.008.

Simonyan, K., and A. Zisserman, 2015: Very deep convolutional networks for large-scale image recognition. arXiv, http://arxiv.org/abs/1409.1556.

Springenberg, J. T., A. Dosovitskiy, T. Brox, and M. Riedmiller, 2015: Striving for simplicity: The all convolutional net. arXiv, http://arxiv.org/abs/1412.6806.

Štěpánek, P., P. Zahradníček, and P. Skalák, 2009: Data quality control and homogenization of air temperature and precipitation series in the area of the Czech Republic in the period

1961–2007. *Adv. Sci. Res.*, **3**, 23–26, https://doi.org/10.5194/asr-3-23-2009.

Tompson, J., R. Goroshin, A. Jain, Y. LeCun, and C. Bregler, 2015: Efficient object localization using convolutional networks. *2015 IEEE Conf. on Computer Vision and Pattern Recognition*, Boston, MA, IEEE, 648–656, https://doi.org/10.1109/CVPR.2015.7298664.

Vandal, T., E. Kodra, S. Ganguly, A. Michaelis, R. Nemani, and A. R. Ganguly, 2018: Generating high resolution climate change projections through single image super-resolution: an abridged version. *Proc. 27th Int. Joint Conf. on Artificial Intelligence*, Stockholm, Sweden, International Joint Conferences on Artificial Intelligence Organization, 5389–5393, https://doi.org/10.24963/ijcai.2018/759.

Wilks, D. S., 2011: *Statistical Methods in the Atmospheric Sciences*. 3rd ed. Elsevier, 676 pp.

Wong, J. S., S. Razavi, B. R. Bonsal, H. S. Wheater, and Z. E. Asong, 2017: Inter-comparison of daily precipitation products for large-scale hydro-climatic applications over Canada. *Hydrol. Earth Syst. Sci.*, **21**, 2163–2185, https://doi.org/10.5194/hess-21-2163-2017.

Xie, P., and P. A. Arkin, 1996: Analyses of global monthly precipitation using gauge observations, satellite estimates, and numerical model predictions. *J. Climate*, **9**, 840–858, https://doi.org/10.1175/1520-0442(1996)009<0840:AOGMPU>2.0.CO;2.

Xu, C.-D., J.-F. Wang, M.-G. Hu, and Q.-X. Li, 2014: Estimation of uncertainty in temperature observations made at meteorological stations using a probabilistic spatiotemporal approach. *J. Appl. Meteor. Climatol.*, **53**, 1538–1546, https://doi.org/10.1175/JAMC-D-13-0179.1.

Yang, D., D. Kane, Z. Zhang, D. Legates, and B. Goodison, 2005: Bias corrections of long-term (1973–2004) daily precipitation data over the northern regions. *Geophys. Res. Lett.*, **32**, L19501, https://doi.org/10.1029/2005GL024057.

You, J., K. G. Hubbard, S. Nadarajah, and K. E. Kunkel, 2007: Performance of quality assurance procedures on daily precipitation. *J. Atmos. Oceanic Technol.*, **24**, 821–834, https://doi.org/10.1175/JTECH2002.1.

Zeiler, M. D., and R. Fergus, 2014: Visualizing and understanding convolutional networks. *13th European Conf. on Computer Vision*, Zurich, Switzerland, ECCV, https://doi.org/10.1007/978-3-319-10590-1_53.

Zhao, Q., Y. Zhu, D. Wan, Y. Yu, and X. Cheng, 2018: Research on the data-driven quality control method of hydrological time series data. *Water*, **10**, 1712, https://doi.org/10.3390/w10121712.